Structural relaxation in dense liquids composed of anisotropic particles

Tianqi Shen, Carl Schreck, Bulbul Chakraborty, Denise E. Freed, and Corey S. O'Hern

Phys. Rev. E **86**, 041303 — Published 10 October 2012

DOI: 10.1103/PhysRevE.86.041303

Structural relaxation in dense liquids composed of anisotropic particles

Tianqi Shen[1], Carl Schreck[1], Bulbul Chakraborty[2], Denise E. Freed[3], and Corey S. O'Hern[4,1]
[1] *Department of Physics, Yale University, New Haven, Connecticut 06520-8120, USA*
[2] *Martin Fisher School of Physics, Brandeis University, Mail Stop 057, Waltham, Massachusetts 02454-9110, USA*
[3] *Schlumberger-Doll Research Center, One Hampshire Street, Cambridge, Massachusetts 02139, USA and*
[4] *Department of Mechanical Engineering & Materials Science, Yale University, New Haven, Connecticut 06520-8286, USA*

We perform extensive molecular dynamics simulations of dense liquids composed of bidisperse dimer- and ellipse-shaped particles in 2D that interact via purely-repulsive contact forces. We measure the structural relaxation times obtained from the long-time α-decay of the self-part of the intermediate scattering function for the translational and rotational degrees of freedom (DOF) as a function of packing fraction ϕ, temperature T, and aspect ratio α. We are able to collapse the packing-fraction and temperature-dependent structural relaxation times for disks, and dimers and ellipses over a wide range of α, onto a universal scaling function $\mathcal{F}_{\pm}(|\phi-\phi_0|,T,\alpha)$, which is similar to that employed in previous studies of dense liquids composed of purely repulsive spherical particles in 3D. $\mathcal{F}_{\pm}$ for both the translational and rotational DOF are characterized by the α-dependent scaling exponents μ and δ and packing fraction $\phi_0(\alpha)$ that signals the crossover in the scaling form $\mathcal{F}_{\pm}$ from hard-particle dynamics to super-Arrhenius behavior for each aspect ratio. We find that the fragility of structural relaxation at ϕ_0, $m(\phi_0)$, decreases monotonically with increasing aspect ratio for both ellipses and dimers. For $\alpha > \alpha_p$, where α_p is the location of the peak in the packing fraction ϕ_J at jamming onset, the rotational DOF are strongly coupled to the translational DOF and the dynamic scaling exponents and ϕ_0 are similar for the rotational and translational DOF. For $1 < \alpha < \alpha_p$, the translational DOF become frozen at higher temperatures than the rotational DOF, and ϕ_0 for the rotational degrees of freedom increases above ϕ_J. Moreover, the results for the slow dynamics of dense liquids composed of dimer- and ellipse-shaped particles are qualitatively the same, despite the fact that zero-temperature static packings of dimers are isostatic, while static packings of ellipses are hypostatic. Thus, zero-temperature contact counting arguments do not apply to structural relaxation of dense liquids of anisotropic particles near the glass transition.

PACS numbers: 05.10.-1,64.70.Pf,83.80.Fg

I. INTRODUCTION

One of the hallmarks of glassy behavior in dense liquids is the rapid increase in the stress and structural relaxation times as the density is increased or the temperature is lowered toward the glass transition [1]. Several recent studies have characterized how the fragility, *i.e.* the rate of increase of the stress and structural relaxation times with decreasing temperature near the glass transition [2], depends on the packing fraction in dense liquids of *spherical* particles that interact via purely repulsive contact potentials [3–6]. In particular, Refs. [5, 6] have shown that for dense liquids composed of bidisperse spheres in three dimensions (3D) the temperature and packing fraction dependence of the structural relaxation time τ can be collapsed onto two master curves, one for $\phi > \phi_0$ and another for $\phi < \phi_0$. For $\phi < \phi_0$, the scaling function reduces to hard-sphere behavior $\tau \sim \exp[A/|\phi_0 - \phi|^{\delta}]$ in the zero-temperature limit ($T \to 0$), where $A > 0$ is a constant and δ is a scaling exponent that does not depend on the form of the repulsive contact potential. For $\phi > \phi_0$, the temperature dependence of the structural relaxation time is super-Arrhenius and the fragility of structural relaxation increases with packing fraction. For 3D bidisperse spheres, $\phi_0 \sim 0.635$, which is distinct from the jammed packing fraction ϕ_J for both fast and slow packing-generation protocols [5–8].

Despite the fact that there have been a number studies of the rapidly growing structural and stress relaxation times near the glass transition in dense liquids composed of *anisotropic* particles [9–14], there have been few quantitative calculations of the fragility of structural relaxation for dense liquids as a function of the particle shape. In this article, we investigate the slow dynamics of both the translational and rotational degrees of freedom in dense amorphous liquids composed of bidisperse dimer- and ellipse-shaped particles in two dimensions (2D) that interact via purely repulsive contact forces as a function of temperature, packing fraction, and aspect ratio.

We address several important questions: 1) What are the forms for the structural relaxation times for the translational and rotational degrees of freedom for dimer- and ellipse-shaped particles as a function of temperature and packing fraction? 2) Can we identify master curves for the structural relaxation times for $\phi > \phi_0(\alpha)$ and $\phi < \phi_0(\alpha)$ for each α similar to those found for spherical particles at $\alpha = 1$? 3) Are the slow dynamics of dense liquids composed of anisotropic, elongated particles more or less fragile near $\phi_0(\alpha)$ than spherical particles? 4) Do differences in microscale geometrical features lead to qualitative changes in structural relaxation in systems composed of anisotropic particles?

To address these questions, we performed extensive molecular dynamics simulations of supercooled liquids composed of frictionless, purely repulsive dimer- and ellipse-shaped particles in 2D over a wide range of temperature T, packing fraction ϕ, and aspect ratio α.

We find four key results. First, we show that the structural relaxation times for dimer- and ellipse-shaped particles in 2D obey scaling forms similar to that for 3D systems composed of bidisperse spheres [5, 6]. In particular, we find that there is an aspect-ratio dependent packing fraction $\phi_0(\alpha)$ below which the structural relaxation time converges to hard-particle behavior in the zero-temperature limit and above which the structural relaxation time grows super-Arrheniusly with decreasing temperature. Second, we identify a universal scaling form $\mathcal{F}_{\pm}(|\phi-\phi_0|,T,\alpha)$ ($\mathcal{F}_-$ for $\phi<\phi_0(\alpha)$ and $\mathcal{F}_+$ for $\phi>\phi_0(\alpha)$) that collapses the structural relaxation times for all 2D particle shapes studied, including bidisperse disks and both dimer- and ellipse-shaped particles over a wide range of α. For small α, the rotational degrees of freedom (DOF) are not 'caged' at temperatures where the translational degrees of freedom become frozen, and $\phi_0(\alpha)$ for the rotational degrees of freedom increases above $\phi_J(\alpha)$. For $\alpha>\alpha_p$ (the location of the peak in $\phi_J(\alpha)$ [15]), the rotational degrees of freedom are strongly coupled to the translational degrees of freedom, and obey scaling functions with similar scaling exponents. Third, the fragility at ϕ_0 of structural relaxation decreases monotonically with increasing aspect ratio for both dimers and ellipses. Finally, we do not find qualitative differences in the slow dynamics of dense liquids composed of dimer- and ellipse-shaped particles, despite the fact that dimer packings at zero temperature are isostatic [16] at jamming onset with on average six contacts per particle in 2D ($z=z_{\rm iso}=6$) for $1<\alpha\leq 2$, whereas ellipse packings at zero temperature are hypostatic with $z<z_{\rm iso}$ over the same range in α [15]. Naively, one might have expected that the structural relaxation times for hypostatic systems decay more quickly than those for isostatic systems at a given packing fraction $|\phi-\phi_J(\alpha)|$ and temperature T. However, we show that counting arguments for zero temperature packings do not apply for dense liquids composed of anisotropic particles near the glass transition.

The organization of the remainder of the article is as follows. In Sec. II, we describe the methods we employed to measure the structural relaxation times for the translational and rotational degrees of freedom for dense liquids composed of anisotropic particles in 2D. As a test of our methods, we show in Sec. II the results for the collapse of the structural relaxation times for dense liquids composed of 2D bidisperse disks onto the scaling form $F_{\pm}(|\phi-\phi_0|,T)$ used in Refs. [5, 6] for 3D bidisperse spheres. In Sec. III, we present our novel results for the structural relaxation times for the rotational and translational degrees of freedom for dimer- and ellipse-shaped particles as a function of temperature, packing fraction, and aspect ratio, and show that the relaxation time data for dimers and ellipses can be collapsed onto a generalized scaling function $\mathcal{F}_{\pm}(|\phi-\phi_0|,T,\alpha)$. In Sec. IV, we summarize our results and identify several important open questions for future research studies. The Appendix includes additional numerical calculations of the system-size dependence of the structural relaxation times and nematic order as a function of temperature and packing fraction that supplement the results in Sec. III.

II. METHODS

We performed molecular dynamics (MD) simulations of systems composed of bidisperse, frictionless rigid dimer- and ellipse-shaped particles with mass m in 2D that interact via purely repulsive contact forces. We chose bidisperse systems, where half of the particles are large with major axis $a_l=1.4$ and half are small with major axis $a_s=1$, to prevent positional and orientational ordering. We varied the aspect ratio (ratio of the major and minor axes) $\alpha=a_l/b_l=a_s/b_s$ in the range $1\leq\alpha\leq 2.2$. (See Fig. 1.) Note that rigid dimers with $\alpha\gtrsim 2$ possess a small gap between pairs of monomers that comprise a given dimer. We employed periodic boundary conditions in a square cell with length L and studied system sizes in the range $N=64$ to 256 particles to assess finite-size effects.

The particles interact via the pairwise, purely repulsive linear spring potential,

$$V(r_{ij})=\frac{\epsilon}{2}\left(1-\frac{r_{ij}}{\sigma_{ij}}\right)^2\Theta\left(1-\frac{r_{ij}}{\sigma_{ij}}\right), \tag{1}$$

where ϵ is the characteristic energy scale of the repulsive interaction, $\Theta(x)$ is the Heaviside step function, so that particles only interact when they overlap, and σ_{ij} is the contact distance between particles i and j that in general depends on the particle orientations and separation vector $\vec{r}_{ij}$. For ellipses, $\vec{r}_{ij}$ connects the centers of mass of ellipses i and j as shown in Fig. 2, while for dimers, $\vec{r}_{ij}$ connects monomers i and j on distinct dimers k and l. For dimers, $\sigma_{ij}=(\sigma_i+\sigma_j)/2$, where σ_i is the diameter of monomer i. The method for calculating the contact distance between two ellipses is discussed in detail in Ref. [17]. Both the large and small ellipses possess the same moment of inertia $I_e=(a_l/a_s)mb^2(1+\alpha^2)/16$, while the small dimers have a moment of inertia $I_{ds}=mb^2(\alpha-1)^2/4$ and large dimers have a moment of inertia $I_{dl}=mb^2(\alpha-1)^2(a_l/2a_s)^2$. We chose ϵ and $b\sqrt{m/\epsilon}$ as the energy and time units.

To prepare the systems at a given temperature, we first solve Newton's equations of motion using the velocity Verlet algorithm with a velocity rescaling thermostat [18] using a time step $\Delta t=0.01$. We then equilibrate and study

the system dynamics without the thermostat in the NVE ensemble. To identify the structural relaxation times, we measure the self-part of the intermediate scattering function (ISF) for the translational degrees of freedom,

$$F_t(q,t) = \frac{1}{N_l}\left\langle \sum_{j=1}^{N_l} e^{i\vec{q}\cdot[\vec{r}_j(t)-\vec{r}_j(0)]} \right\rangle, \tag{2}$$

where the wavenumber $q = 2\pi/a_l$, $N_l = N/2$ is the number of large particles, and $\langle\cdot\rangle$ indicates an average over the orientations of $\vec{q}$ and time origins. To quantify relaxation of the rotational degrees of freedom, we calculated

$$F_r(n,t) = \frac{1}{N_l}\left\langle \sum_{j=1}^{N_l} e^{in[\theta_j(t)-\theta_j(0)]} \right\rangle, \tag{3}$$

where θ_i is the angle between the orientation $\hat{u}_i$ of particle i and the horizontal axis and $\langle\cdot\rangle$ indicates an average over time origins. For most studies, we focused on $n = 1$, in which case relaxation of the ISF occurs when the dimer- or ellipse-shaped particles flip by π.

We measured the structural relaxation times for dense liquids composed of bidisperse disks, dimer-, and ellipse-shaped particles over a wide range in packing fraction from 0.75 to 0.94, temperature from 10^{-2} to 10^{-6}, and aspect ratio $1 < \alpha < 2$. In this regime, the ISF for the translational and rotational degrees of freedom display stretched exponential relaxation

$$F_t(q,t) \approx C_t e^{-(t/\tau_t)^{\beta_t}} \tag{4}$$

$$F_r(1,t) \approx C_r e^{-(t/\tau_r)^{\beta_r}} \tag{5}$$

at long times in the α-decay regime, where C_t and C_r are prefactors, β_t and β_r are the stretching exponents, and τ_t and τ_r are characteristic relaxation times for the translational and rotational degrees of freedom, respectively. In Fig. 3 we show the ISF for the translational degrees of freedom for bidisperse disks in 2D with fits to the stretched exponential form (Eq. 4) at long times. We find that the stretching exponent β_t decreases with increasing packing fraction and decreasing temperature (lower inset to Fig. 3). In Sec. III, we will show results from measurements of the decay of the self-part of the intermediate scattering function for both the translational and rotational degrees of freedom for dimer- and ellipse-shaped particles as a function of ϕ, T, and α. Prior to all measurements, we run MD simulations of the system for 10 times the longest relaxation time τ to reach metastable equilibrium.

We also monitor the positional and orientational ordering of the systems as a function of decreasing temperature by measuring the bond orientational order [19] and nematic order parameter

$$P_2 = \langle 2\cos^2(\theta_i - \overline{\theta}) - 1\rangle, \tag{6}$$

where $\overline{\theta}$ is the average particle orientation in a given configuration and the angle brackets indicate an average over independent configurations. As shown in the snapshots of the configurations in Fig. 4, we do not find significant positional or orientational ordering in dense liquids of bidisperse dimer- and ellipse-shaped particles.

In previous studies of slow dynamics in dense liquids, Witten and Berthier [5] identified a dynamical scaling relation,

$$\tau(\phi,T)\sqrt{T} \sim \exp\left[\frac{A}{|\phi_0-\phi|^{\delta}} F_{\pm}\left(\frac{|\phi_0-\phi|^{2/\mu}}{T}\right)\right], \tag{7}$$

which collapsed the structural relaxation time $\tau(\phi,T)$ from the self-part of the intermediate scattering function for bidisperse, purely repulsive spheres in 3D over a wide range of temperature and packing fraction. The scaling function $F_{\pm}$ assumes two different forms above and below $\phi_0 \sim 0.635$, and is only a function of $|\phi_0-\phi|^{2/\mu}/T$, where μ is an exponent that controls the scaling of the potential energy with temperature, $V \approx V_0 T^{\mu}$, near ϕ_0. These studies showed that τ_t displays hard-sphere dynamics in the zero-temperature limit for $\phi < \phi_0$, but τ_t displays super-Arrhenius behavior with decreasing temperature for $\phi > \phi_0$. For $\phi \to \phi_0$, $x \equiv |\phi_0-\phi|^{2/\mu}/T \ll 1$ and $F_{\pm}(x) \sim x^{\delta\mu/2}$, which implies that $\tau \sim \exp(A/T^{\mu\delta/2})$ and the fragility $m(\phi_0) = \mu\delta/2$ of structural relaxation at ϕ_0 for $T \to 0$ is controlled by the scaling exponents μ and δ. The scaling exponent δ does not depend of the form of the purely repulsive contact potential. The results for the scaling exponents μ and δ, ϕ_0, and fragility $m(\phi_0)$ of structural relaxation from Ref. [5] are shown in Table I for dense liquids composed of bidisperse, purely repulsive spheres in 3D.

In Ref. [5], Berthier and Witten also compared the critical packing fraction $\phi_0 \sim 0.635$ (which signals the crossover from hard-sphere dynamics to super-Arrhenius temperature dependence of τ) to the packing fraction ϕ_J at jamming onset. Numerous studies have shown that ϕ_J for frictionless, purely repulsive spherical particles depends on control parameters in the jammed packing-generation protocol (*e.g.* the compression and energy dissipation rates) [8, 20–22]

as shown schematically in Fig. 5. In the limit of infinitely fast rates, the most dilute and disordered mechanically stable packings at ϕ_J^f are obtained. In contrast, in the limit of infinitely slow rates, the densest crystalline packings are obtained. At finite rates, intermediate values of the packing fraction at jamming onset and positional and other types of order can be obtained. Previous studies have shown for bidisperse systems that disordered mechanically stable packings at jamming onset can exist over a finite range of packing fractions (*i.e.* from ϕ_J^f to ϕ_J^s in Fig. 5) with only small and subtle changes in positional order. For 3D bidisperse spheres, $\phi_J^f \approx 0.648$ [7] and $\phi_J^s \approx 0.662$ [5]. The scaling analyses in Refs. [5, 6] for the structural relaxation times for 3D bidisperse systems suggest that $\phi_0 < \phi_J^f$.

Recent experimental [23, 24] and computational [15, 25] studies have shown that the average jammed packing fraction (in the limit of fast quenching rates) $\phi_J(\alpha)$ for static packings of anisotropic frictionless particles increases with aspect ratio α from 'random close packing' [26] at $\alpha = 1$, reaches a peak near $\alpha_p \sim 1.5$ (where α_p depends on the specific particle shape and spatial dimension), and decreases continuously beyond α_p. (See Fig. 7 for a plot of the jammed packing fraction $\phi_J(\alpha)$ for ellipses and dimers as a function of aspect ratio in two dimensions (2D).) In these studies, the jammed packings were created using 'fast' packing-generation protocols, and thus these packings do not possess significant positional or orientational order [17, 27, 28].

III. SCALING ANALYSIS FOR THE STRUCTURAL RELAXATION TIMES

In this section, we describe our measurements of the structural relaxation time τ from the self-part of the intermediate scattering function for the translational and rotational degrees of freedom for bidisperse disks, dimer- and ellipse-shaped particles. We will investigate the extent to which the scaling relation in Eq. 7 holds for 2D systems as a function of aspect ratio and determine the variation with aspect ratio of the fragility of structural relaxation at $\phi_0(\alpha)$ that signals the crossover from hard-particle dynamics to super-Arrhenius temperature dependence. We find no significant positional or nematic ordering with decreasing temperature over the full range of packing fraction and aspect ratio. (See Fig. 16 that shows the nematic order parameter $P_2 \lesssim 1/\sqrt{N}$ for $\alpha = 1.8$ ellipses over a wide range of packing fraction and temperature.)

We first focus on the slow dynamics of dense liquids composed of bidisperse disks in 2D near jamming to compare our results with those obtained for dense 3D liquids of bidisperse spheres [5, 6]. The structural relaxation time τ_t obtained from the self-part of the intermediate scattering function is plotted versus the inverse temperature $1/T$ in Fig. 6 (a) over a wide range in packing fraction from $\phi = 0.75$ to 0.94. One can clearly identify a change in the form of the structural relaxation time as the packing fraction increases above $\phi_0 \approx 0.82 - 0.84$. In Fig. 6 (b), we collapse the data in (a) using the scaling form in Eq. 7 by plotting $|\phi_0 - \phi|^\delta \ln(\tau_t\sqrt{T})$ versus $|\phi_0 - \phi|^{2/\mu}/T$. The exponent μ is obtained from the power-law scaling of the total potential energy V with temperature for $\phi \approx \phi_0$ [5, 6]. In the inset to Fig. 6 (b), we show that $V \sim T^\mu$ over several orders of magnitude in temperature with an exponent $\mu = 1.25$, which is similar to the corresponding value for 3D bidisperse spheres, $\mu_{3D} = 1.3$ [5]. The scaling form for the structural relaxation time possesses two distinct branches: F_+ for $\phi > \phi_0$ and F_- for $\phi < \phi_0$. To obtain Fig. 6 (b), we chose the combination of parameters $\phi_0 = 0.831$, $\mu(\phi_0) = 1.25$, and $\delta = 1.19$ that yielded the tightest collapse of the τ_t data in Fig. 6 (a). For 2D bidisperse systems, we find that the fragility of structural relaxation at ϕ_0, $m(\phi_0) = 1.2$, which is slightly lower than the comparable value, $m(\phi_0) = 1.4$, for 3D bidisperse spheres. (See Table I.)

In Figs. 8 and 9, we show the ISF for the translational and rotational degrees of freedom for dimers and ellipses, respectively, over a range of temperatures at comparable values of the packing fraction $\phi - \phi_J(\alpha)$ for aspect ratio $\alpha = 1.6$ above α_p at which the peak in $\phi_J(\alpha)$ occurs (Fig. 7). For both dimers and ellipses, the decay of the ISF for the translational and rotational degrees of freedom at long-times can be described using a stretched exponential form as shown in Fig 10. For $\alpha \gtrsim \alpha_p$ the rotational degrees of freedom are strongly coupled to the translational degrees of freedom and $\tau_r \sim \tau_t$. For both dimers and ellipses, the 'plateau' value of the ISF is larger for the rotational degrees of freedom compared to that for the translational degrees of freedom. The only significant difference between the intermediate scattering functions for dimers and ellipses in Figs. 8 and 9 is that the plateau value for the translational degrees of freedom is smaller ($F_t \sim 0.6$ - 0.7) compared to that for dimers ($F_t \sim 0.95$), which indicates that the 'cage' size for ellipses is larger than that for dimers.

We use a similar procedure to that employed for bidisperse disks to collapse the data for the structural relaxation times τ_r and τ_t for dimer- and ellipse-shaped particles using the scaling form in Eq. 7. Examples of the collapse of the structural relaxation times for the translational degrees of freedom for dimers and ellipses are shown in Figs. 11 and 12, respectively, at aspect ratio $\alpha = 1.8$. Similar collapse for τ_r is found for both dimer- and ellipse-shaped particles. Also, the quality of the data collapse is the same for dimers and ellipses. We plot the characteristic packing fraction $\phi_0(\alpha)$ that signals the change in scaling form for $\tau(\phi, T)$, the scaling exponents μ and δ, and the fragility $m(\phi_0)$ for the rotational and translational degrees of freedom as a function of aspect ratio α for dimers and ellipses in Figs. 13 and 14, respectively.

For dimers, the fragility $m(\phi_0)$ for the translational degrees of freedom decreases by a factor of ≈ 2.5 with increasing aspect ratio from $m(\phi_0) \approx 1.2$ at $\alpha = 1$ to ≈ 0.5 at $\alpha = 1.8$. The decrease in fragility of structural relaxation is caused by the decrease in the scaling exponent δ (and thus insensitive to the form of the purely repulsive contact forces) because $\mu \sim 1.25$ is nearly constant over this range in aspect ratio. The fragility for the rotational degrees of freedom decreases by a similar factor to that for the translational degrees of freedom for $\alpha \geq 1.2$. In addition, in Fig. 13 (a) we show that the α-dependence of ϕ_0 for the translational degrees of freedom matches that for ϕ_J, *i.e.* nonmonotonic dependence on α with a peak near $\alpha_p \approx 1.4$, and ϕ_0 satisfies $\phi_0(\alpha) < \phi_J(\alpha)$. For $\alpha \geq \alpha_p$, ϕ_0 is the same for the translational and rotational degrees of freedom. However, for $\alpha < \alpha_p$, ϕ_0 for the rotational degrees of freedom increases with decreasing α and becomes larger than ϕ_0 for the translational degrees of freedom and ϕ_J. This strong increase in ϕ_0 for the rotational degrees of freedom at small α indicates the existence of a 'rotator', amorphous, solid-like regime [29] at low temperatures, where the translational degrees of freedom are frozen, but the rotational degrees of freedom are liquid-like. We show that these results are nearly independent of system size by comparing the scaling collapse of the structural relaxation times for the translational degrees of freedom for systems composed of $N = 64$ and 200 dimers at aspect ratio $\alpha = 1.3$ in Fig. 17.

We find quantitatively similar behavior for the dependence of the scaling exponents μ and δ, fragility $m(\phi_0)$ of structural relaxation, and packing fraction ϕ_0 on aspect ratio for ellipses and dimers as shown in Fig. 14. A minor difference between dimers and ellipses is the weaker decrease in ϕ_0 and ϕ_J with increasing aspect ratio α. Again, ϕ_0 for the rotational degrees of freedom increases above ϕ_0 for the translational degrees of freedom and ϕ_J for $\alpha \lesssim \alpha_p$, which indicates the onset of the 'rotator' regime for low aspect ratios. In Fig. 15 we show that we are able to collapse all of the structural relaxation time data for the translational and rotational degrees of freedom for bidisperse dimers and ellipses using the generalized scaling form

$$\mathcal{F}_{\pm}(x) = c(\alpha)[F_{\pm}(x)]^{1/m(\phi_0(\alpha))}, \tag{8}$$

where $c(\alpha)$ is an α-dependent prefactor that is different for the translational and rotational degrees of freedom and $x \equiv |\phi - \phi_0|^{2/\mu}/T$. Thus, we find that the scaling behavior of the structural relaxation times for dimers and ellipses is nearly identical over a wide range of aspect ratios, despite the fact that static packings of dimer-shaped particles are isostatic while static packings of ellipse-shaped particles are hypostatic at zero temperature.

IV. CONCLUSIONS

We performed extensive molecular dynamics simulations of the slow dynamics in dense liquids composed of bidisperse, purely repulsive dimer- and ellipse-shaped particles in 2D. We showed that a similar scaling form to that identified for structural relaxation for spherical particles [5, 6] is able to collapse the packing fraction and temperature-dependent structural relaxation times for the rotational and translational degrees of freedom for dimer- and ellipse-shaped particles over a wide range of aspect ratios α (Fig. 15). Thus, the dynamical critical point at $T = 0$ and $\phi = \phi_0$ studied in Refs. [5, 6] for dense liquids composed of purely repulsive spheres can be generalized to $T = 0$, $\phi = \phi_0$, and $\alpha = 1$, and this dynamical critical point controls the temperature, packing fraction, and aspect-ratio-dependent fragility of structural relaxation for dense liquids composed of dimer- and ellipse-shaped particles. Furthermore, we find qualitatively and quantitatively similar results for the dynamical scaling exponents, packing fraction ϕ_0 that signals the crossover from hard-particle dynamics to super-Arrhenius temperature dependence, and fragility $m(\phi_0)$ of structural relaxation for dimer- and ellipse-shaped particles. In particular, for dimers and ellipses the fragility of structural relaxation at ϕ_0 decreases monotonically with increasing aspect ratio. Thus, the microscale differences in shape between dimers and ellipses do not give rise to important differences in the slow dynamics of structural relaxation in dense supercooled liquids of anisotropic particles. In contrast, static packings of dimers at zero temperature are isostatic, while static packings of ellipses are hypostatic, which leads to significant differences in the density of vibrational modes and static shear modulus at zero temperature [17, 27].

These findings suggest several important future studies. First, we will investigate possible causes of the decrease in fragility of structural relaxation for dense liquids composed of elongated particles with increasing aspect ratio, including an increase in the number of inherent structures [30] and vibrational entropy [1] with increasing α. Second, we will determine whether the temperature, packing fraction, and aspect ratio dependence of the shear viscosity and inverse diffusion coefficient for dimers and ellipses obeys the same scaling form as that found for the structural relaxation time [31, 32]. Third, is there a nonequilibrium, finite-temperature regime where microscale differences between anisotropic particle shapes can cause significant differences in the time-dependent structural and mechanical response of the system? To address this question, we will subject jammed packings of dimers and ellipses to weak thermal fluctuations (much below the temperatures studied in the present manuscript) and measure the time-dependent structural and stress relaxation.

Acknowledgments

Support from NSF grant numbers DMR-0905880 (BC), DMS-0835742 (TS and CO), DMR-1006537 (TS and CO), and the Raymond and Beverly Sackler Institute for Biological, Physical, and Engineering Sciences (TS) is acknowledged. This work also benefited from the facilities and staff of the Yale University Faculty of Arts and Sciences High Performance Computing Center and NSF Grant No. CNS-0821132 that partially funded acquisition of the computational facilities. BC also acknowledges the hospitality of the Schlumberger-Doll Research Center where part of this work was performed.

Appendix A: Supplementary Results

In this section, we provide additional numerical calculations that supplement the results presented in Sec. III. In Fig. 16, we show the average nematic order P_2 (Eq. 6) for dense liquids composed of ellipses with $\alpha = 1.8$ versus $1/T$ over a wide range of packing fractions above and below ϕ_0. $P_2 \lesssim 1/\sqrt{N}$ for all systems studied, which indicates that the ellipse orientations are disordered. We obtain similar results to those in Fig. 16 for dense liquids of bidisperse dimers over the range of T, ϕ, and α considered.

In Fig. 17, we investigate the effect of system size on the structural relaxation times. We show that the scaled structural relaxation times for the translational degrees of freedom for dense liquids composed of dimers for two system sizes ($N = 64$ and 200) are nearly identical. Similar results to those in Fig. 17 for dimers hold over the full range of aspect ratio considered. We also find that there are negligible system-size effects for the structural relaxation times for ellipses with $N \geq 64$ for $1 < \alpha < 2$.

[1] P. G. Debenedetti and F. H. Stillinger, *Nature* **410** (2001) 259.
[2] C. A. Angell, *Science* **267** (1995) 1924.
[3] M. Schmiedeberg, T. K. Haxton, S. R. Nagel, and A. J. Liu, *Europhys. Lett.* **96** (2011) 36010.
[4] T. K. Haxton, M. Schmiedeberg, and A. J. Liu, *Phys. Rev. E* **83** (2011) 031503.
[5] L. Berthier and T. A. Witten, *Europhys. Lett.* **86** (2009) 10001.
[6] L. Berthier and T. A. Witten, *Phys. Rev. E* **80** (2009) 021502.
[7] C. S. O'Hern, L. E. Silbert, A. J. Liu, and S. R. Nagel, *Phys. Rev. E* **68** (2003) 011306.
[8] C. F. Schreck, C. S. O'Hern, and L. E. Silbert, *Phys. Rev. E* **84** (2011) 011305.
[9] M. Letz, R. Schilling, and A. Latz, *Phys. Rev. E* **62** (2000) 5173.
[10] P. Pfleiderer, K. Kilinkovic, and T. Schilling, *Europhys. Lett.* **84** (2008) 16003.
[11] R. Zhang and K. S. Schweizer, *J. Chem. Phys.* **133** (2010) 104902.
[12] S. Kammerer, W. Kob, and R. Schilling, *Phys. Rev. E* **56** (1997) 5450.
[13] S. Kammerer, W. Kob, and R. Schilling, *Phys. Rev. E* **58** (1998) 2131.
[14] S. Kammerer, W. Kob, and R. Schilling, *Phys. Rev. E* **58** (1998) 2141.
[15] C. F. Schreck, N. Xu, and C. S. O'Hern, *Soft Matter* **6** (2010) 2960.
[16] A. V. Tkachenko and T. A. Witten, *Phys. Rev. E* **60** (1999) 687.
[17] C. F. Schreck, M. Mailman, B. Chakraborty, and C. S. O'Hern, *Phys. Rev. E* **85** (2012) 061305.
[18] M. P. Allen and D. J. Tildesley, *Computer Simulations of Liquids* (Oxford University Press, New York, 1987).
[19] P. J. Steinhardt, D. R. Nelson, and M. Ronchetti, *Phys. Rev. B* **28** (1983) 784.
[20] P. Chaudhuri, L. Berthier, and S. Sastry, *Phys. Rev. Lett.* **104** (2010) 165701.
[21] D. Vågberg, P. Olsson, and S. Teitel, *Phys. Rev. E* **83** (2011) 031307.
[22] M. P. Ciamarra, M. Nicodemi, and A. Coniglio, *Soft Matter* **6** (2010) 2871.
[23] W. N. Man, A. Donev, F. H. Stillinger, M. T. Sullivan, W. B. Russel, D. Heeger, S. Inati, S. Torquato, and P. M. Chaikin, *Phys. Rev. Lett.* **94** (2005) 198001.
[24] A. Donev, I. Cisse, D. Sachs, E. A. Variano, F. H. Stillinger, R. Connelly, S. Torquato, and P. M. Chaikin, *Science* **303** (2004) 990.
[25] A. Donev, R. Connelly, F. H. Stillinger and S. Torquato, *Phys. Rev. E* **75** (2007) 051304.
[26] J. G. Berryman, *Phys. Rev. A* **27** (1983) 1053.
[27] M. Mailman, C. F. Schreck, C. S. O'Hern, and B. Chakraborty, *Phys. Rev. Lett.* **102** (2009) 255501.
[28] Z. Zeravcic, N. Xu, A. J. Liu, S. R. Nagel, and W. an Saarloos, *Europhys. Lett.* **87** (2009) 26001.
[29] C. De Michele, R. Schilling, and F. Sciortino, *Phys. Rev. Lett.* **98** (2007) 265702.
[30] S. Sastry, *Nature* **409** (2000) 164.
[31] D. N. Perera and P. Harrowell, *J. Chem. Phys.* **111** (1999) 5441.
[32] D. N. Perera and P. Harrowell, *Phys. Rev. Lett.* **81** (1998) 120.

Figures

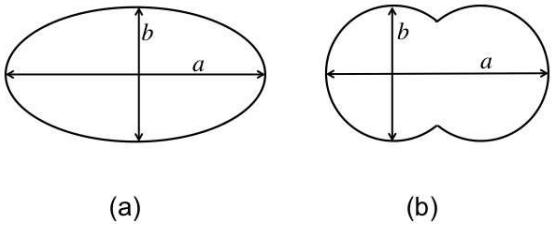

FIG. 1: Definition of the aspect ratio $\alpha = a/b$, where a and b are the length of the major and minor axes, for (a) ellipses and (b) dimers

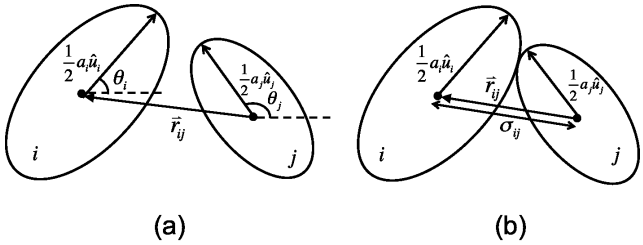

FIG. 2: (a) Schematic of ellipses i and j with orientations $\hat{u}_i$ and $\hat{u}_j$, respectively, and interparticle separation vector $\vec{r}_{ij}$. θ_i is the angle between $\hat{u}_i$ and the horizontal axis. (b) Definition of the contact distance σ_{ij} between ellipses i and j, which is obtained by moving ellipse i toward j along $\hat{r}_{ij}$ while fixing their orientations until they are in contact.

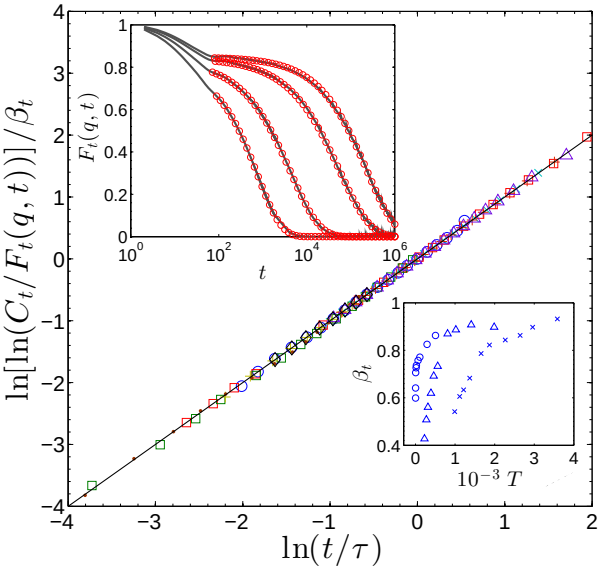

FIG. 3: (Color online) Plot of the scaled self-part of the intermediate scattering function $\ln[\ln(C_t/F_t(q,t))]/\beta_t$ for the translational degrees of freedom (symbols) versus $\ln(t/\tau_t)$, where C_t is the prefactor, β_t is the stretching exponent, and τ_t is the characteristic relaxation time obtained from fits to Eq. 4 for bidisperse disks for packing fractions from 0.78 to 0.90 and temperature from 1.5×10^{-6} to 2×10^{-3}. The solid line has slope 1. (Inset, top) $F_t(q,t)$ versus t (gray lines) with fits (symbols) to the stretched exponential form in Eq. 4 in the long-time α-decay regime for $\phi = 0.83$ and temperatures $T = 5 \times 10^{-4}$, 4.5×10^{-4}, 3×10^{-4}, and 2.5×10^{-4} from left to right. (Inset, bottom) The stretching exponent β_t from fits of $F_t(q,t)$ to Eq. 4 as a function of temperature T at $\phi = 0.78$ (circles), 0.83 (triangles), and 0.90 (crosses).

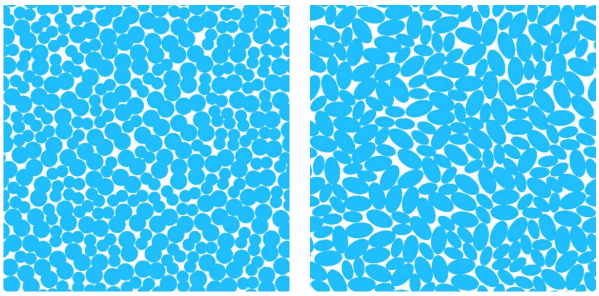

FIG. 4: (Color online) Snapshots of dense liquid configurations of bidisperse dimer- (left) and ellipse-shaped particles (right) with aspect ratio $\alpha = 1.8$, packing fraction $\phi = 0.82$, and temperature $T \approx 5 \times 10^{-5}$.

FIG. 5: Schematic of the possible packing fractions at jamming onset ϕ_J (shaded region) that can be obtained as a function of control parameters in packing-generation protocols (*e.g.* compression or energy dissipation rates), where $\phi_J^f < \phi_j^s < \phi_J^{\rm xtal}$. The most dilute static packings at ϕ_J^f are obtained for infinitely fast quenches, while the densest static packings at $\phi_J^{\rm xtal}$ (with either complex unit cells or phase-separated packings for bidisperse systems) are obtained for infinitely slow quenches. At finite rates, static packings with intermediate packing fraction ϕ_J^s can be obtained. Note that the current studies and those in Refs. [5, 6] indicate that $\phi_0 < \phi_J^f$.

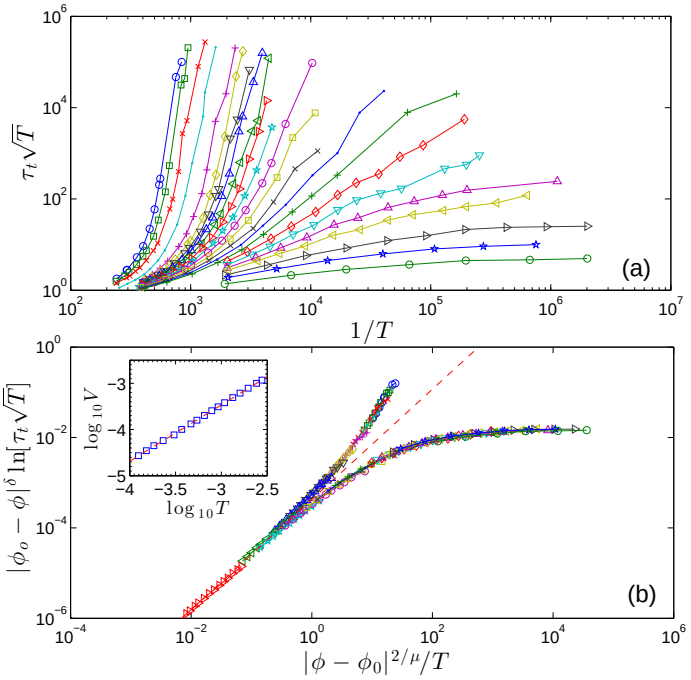

FIG. 6: (Color online) (a) Structural relaxation time $\tau_t\sqrt{T}$ versus $1/T$ for dense liquids of bidisperse disks in 2D for 23 different packing fractions, $\phi = 0.94$, 0.92, 0.90, 0.88, 0.86, 0.85, 0.845, 0.84, 0.835, 0.83, 0.825, 0.82, 0.815, 0.81, 0.805, 0.80, 0.795, 0.79, 0.785, 0.78, 0.77, 0.76, and 0.75 from left to right. (b) Collapse of the data in (a) using Eq. 7 with $\phi_0 = 0.831, \mu = 1.25$, and $\delta = 1.95$. The dashed line has slope $\mu\delta/2$. Inset: Scaling relation between the total potential energy and temperature $V = V_0 T^\mu$ at $\phi = \phi_0 \approx 0.83$, where $V_0 = 2.0$ and $\mu = 1.25$. The dashed line has slope 1.25.

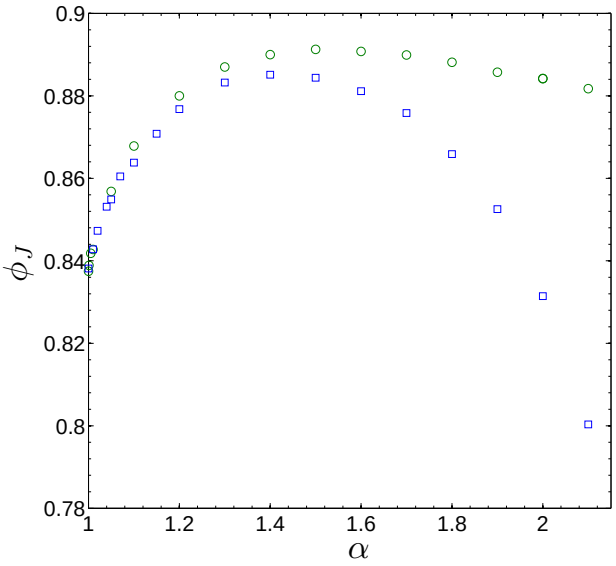

FIG. 7: (Color online) Ensemble averaged packing fraction ϕ_J at jamming onset versus aspect ratio α for $N = 480$ bidisperse, frictionless dimer- (squares) and ellipse-shaped (circles) particles.

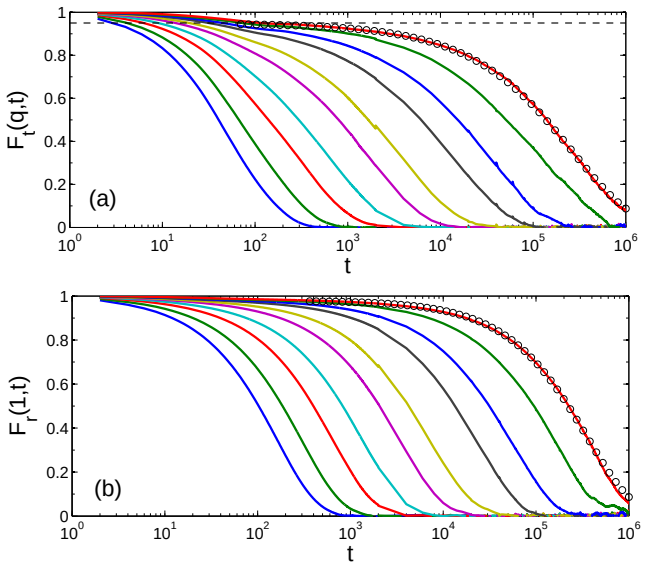

FIG. 8: (Color online) Self-part of the intermediate scattering function (ISF) for the (a) translational and (b) rotational ($n = 1$) degrees of freedom for *dimers* at aspect ratio $\alpha = 1.6$ and packing fraction $\phi = 0.86$ over a range of temperatures $T = 2.5\times10^{-3}$, 1.6×10^{-3}, 1.1×10^{-3}, 7×10^{-4}, 4.6×10^{-4}, 3.1×10^{-4}, 2×10^{-4}, 1.3×10^{-4}, 9×10^{-5} and 1.2×10^{-4} from left to right. The dashed horizontal line in (a) indicates the approximate value of the plateau in the ISF. The symbols in (a) and (b) show fits of the ISF to stretched exponential behavior (Eqs. 4 and 5) for long times.

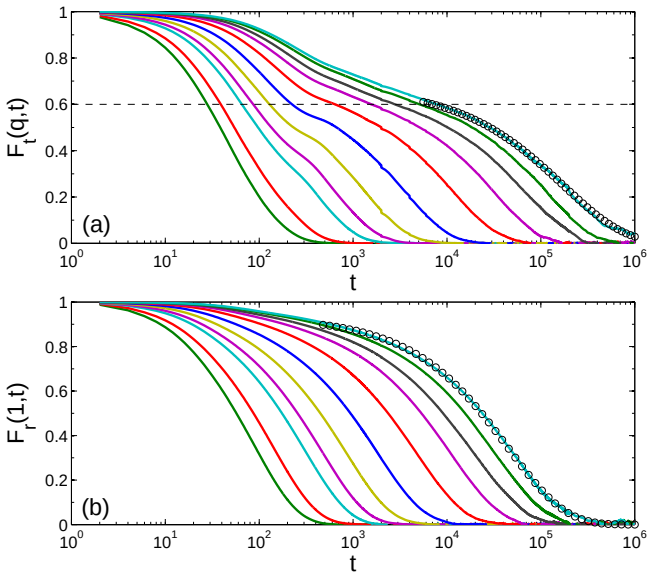

FIG. 9: (Color online) Self-part of the intermediate scattering function for the (a) translational and (b) rotational degrees of freedom ($n = 1$) for *ellipses* at aspect ratio $\alpha = 1.6$ and packing fraction $\phi = 0.87$ over a range of temperature $T = 2 \times 10^{-3}$, 1.5×10^{-3}, 9×10^{-4}, 7×10^{-4}, 5×10^{-4}, 3.1×10^{-4}, 1.8×10^{-4}, 1.6×10^{-4}, 8.5×10^{-5}, 1.2×10^{-4}, and 1.0×10^{-4} from left to right. The dashed horizontal line in (a) indicates the approximate value of the plateau in the ISF. The symbols in (a) and (b) show fits of the ISF to stretched exponential behavior (Eqs. 4 and 5) for long times.

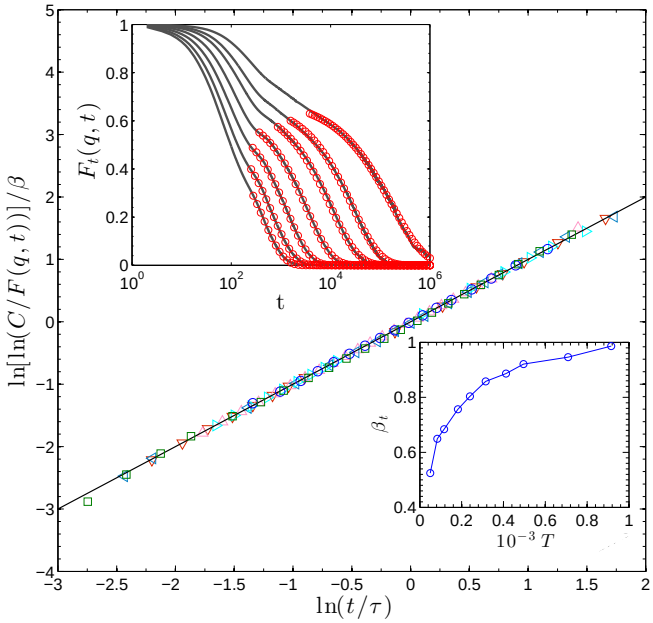

FIG. 10: (Color online) Plot of the scaled self-part of the intermediate scattering function $\ln[\ln(C/F(q,t))]/\beta$ for the translational and rotational degrees of freedom (symbols) versus $\ln(t/\tau)$, where C is the prefactor, β is the stretching exponent, and τ is the characteristic relaxation time obtained from fits to Eqs. 4 and 5 for ellipses and dimers at packing fraction $\phi = 0.87$ over a range of temperature from 10^{-3} to 5×10^{-5}. The solid line has slope 1. (Inset, top) $F_t(q,t)$ versus t (gray lines) with fits (symbols) to the stretched exponential form in Eq. 4 in the long-time α-decay regime for ellipses at $\phi = 0.87$ and temperatures $T = 9 \times 10^{-4}$, 7×10^{-4}, 5×10^{-4}, 3.1×10^{-4}, 1.8×10^{-4}, 1.6×10^{-4}, and 5×10^{-5} from left to right. (Inset, bottom) The stretching exponent β_t from fits of $F_t(q,t)$ to Eq. 4 as a function of temperature T at $\phi = 0.87$ (circles) for ellipses.

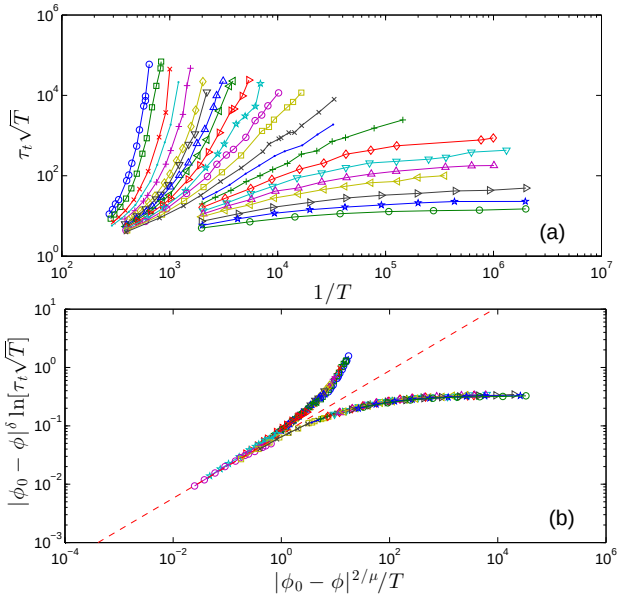

FIG. 11: (Color online) (a) Structural relaxation time for the translational degrees of freedom $\tau_t\sqrt{T}$ as a function of inverse temperature $1/T$ on a ln-ln scale for dimers at aspect ratio $\alpha = 1.8$ over a range of packing fractions $\phi = 0.95$, 0.93, 0.91, 0.90, 0.89, 0.88, 0.875, 0.87, 0.865, 0.86, 0.855, 0.85, 0.845, 0.84, 0.835, 0.83, 0.825, 0.82, 0.815, 0.81, 0.80, 0.79, and 0.78 from left to right. (b) Collapse of the data in (a) using Eq. 7 with $\phi_0 = 0.852, \mu = 1.29$, and $\delta = 0.85$. The dashed line has slope $\mu\delta/2$.

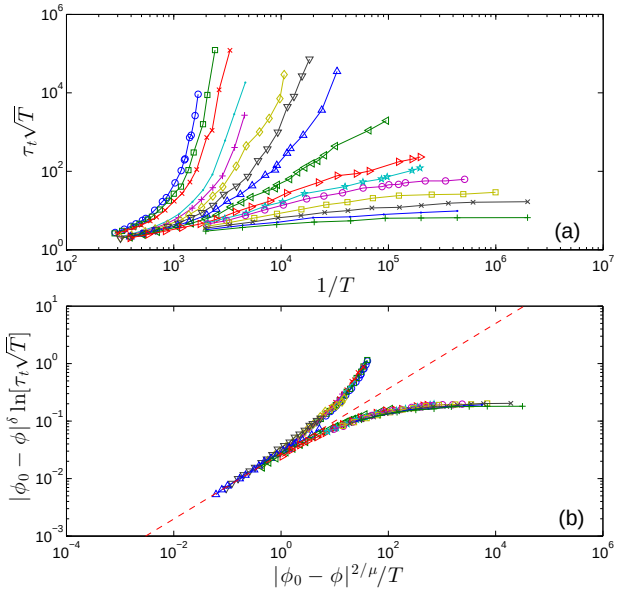

FIG. 12: (Color online) (a) Structural relaxation time for the translational degrees of freedom $\tau_t\sqrt{T}$ as a function of inverse temperature $1/T$ on a ln-ln scale for ellipses at aspect ratio $\alpha = 1.8$ over a range of packing fractions $\phi = 0.98$, 0.96, 0.94, 0.92, 0.91, 0.90, 0.89, 0.88, 0.87, 0.86, 0.855, 0.85, 0.84, 0.83, 0.82, and 0.81 from left to right. (b) Collapse of the data in (a) using Eq. 7 with $\phi_0 = 0.884, \mu = 1.26$, and $\delta = 0.90$. The dashed line has slope $\mu\delta/2$.

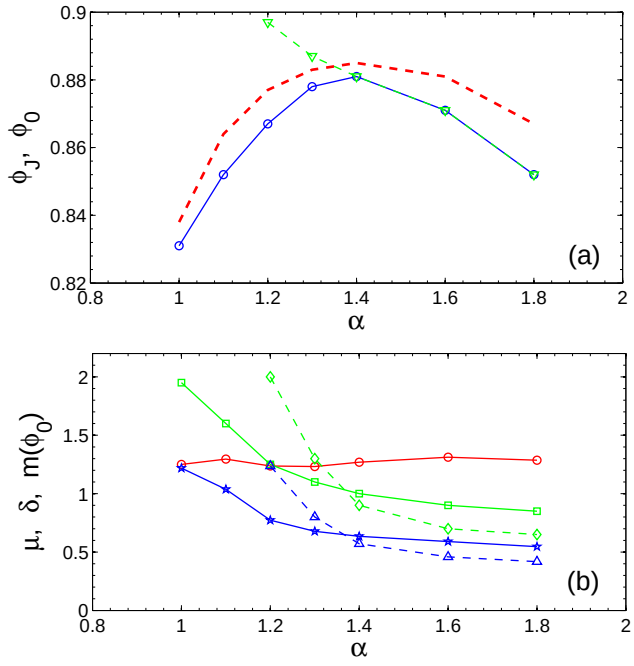

FIG. 13: (Color online) (a) The characteristic packing fraction ϕ_0 that signals the crossover from hard-particle dynamics to super-Arrhenius temperature dependence for the structural relaxation times for the translational (circles) and rotational (downward triangles) degrees of freedom and the packing fraction ϕ_J at jamming onset (dashed line) for dimers as a function of aspect ratio α. (b) The scaling exponents μ (circles, solid line) and δ for translational (squares, solid line) and rotational (diamonds, dashed line) degrees of freedom, and fragility $m(\phi_0)$ for the translational (asterisks, solid line) and rotational (triangles, dashed line) degrees of freedom for dimers versus aspect ratio α.

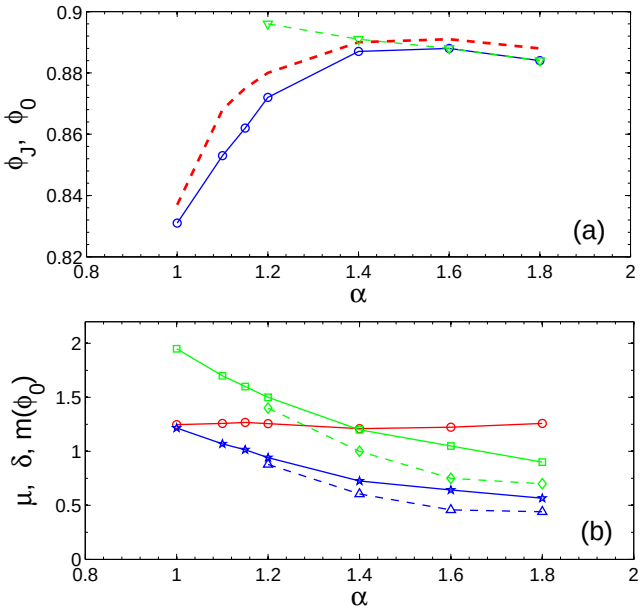

FIG. 14: (Color online) (a) The characteristic packing fraction ϕ_0 that signals the crossover from hard-particle dynamics to super-Arrhenius temperature dependence for the structural relaxation times for the translational (circles) and rotational (downward triangles) degrees of freedom and the packing fraction ϕ_J at jamming onset (dashed line) for ellipses as a function of aspect ratio α. (b) The scaling exponents μ (circles, solid line) and δ for translational (squares, solid line) and rotational (diamonds, dashed line) degrees of freedom, and fragility $m(\phi_0)$ for the translational (asterisks, solid line) and rotational (triangles, dashed line) degrees of freedom for ellipses versus aspect ratio α.

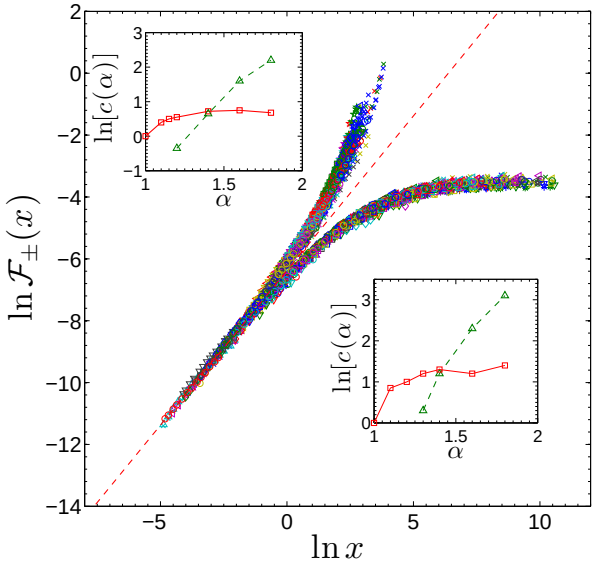

FIG. 15: (Color online) The scaling function $\mathcal{F}_{\pm}(x)$ defined in Eq. 8 versus $x \equiv |\phi - \phi_0|^{2/\mu}/T$, that collapses the structural relaxation times for the translational (Figs. 11 (b) and 12 (b)) and rotational degrees of freedom for ellipses and dimers over a wide range of aspect ratios. The dashed line has slope 1. Insets: $c(\alpha)$ for the translational (solid) and rotational (dashed) degrees of freedom for ellipses (top) and dimers (bottom).

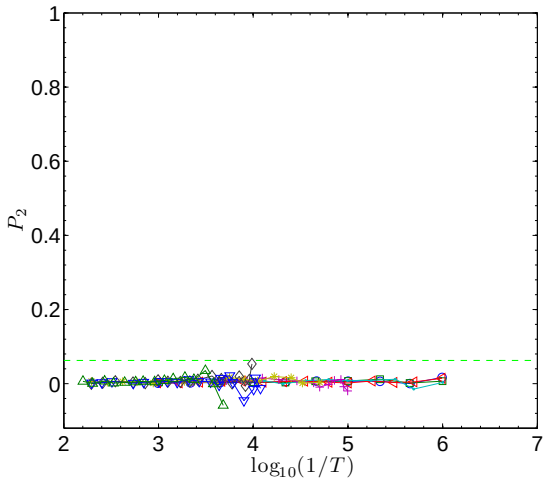

FIG. 16: (Color online) Nematic order parameter P_2 versus $\log_{10}(1/T)$ for dense liquids composed of $N = 200$ ellipses at aspect ratio $\alpha = 1.8$ averaged over 100 configurations for a range of packing fractions $\phi = 0.81$ (open circles), 0.82 (squares), 0.83 (leftward triangles), 0.84 (filled circles), 0.85 (pluses), 0.86 (asterisks), 0.87 (diamonds), 0.88 (downward triangles), and 0.90 (upward triangles). The dashed horizontal line indicates $P_2 = 1/\sqrt{N}$.

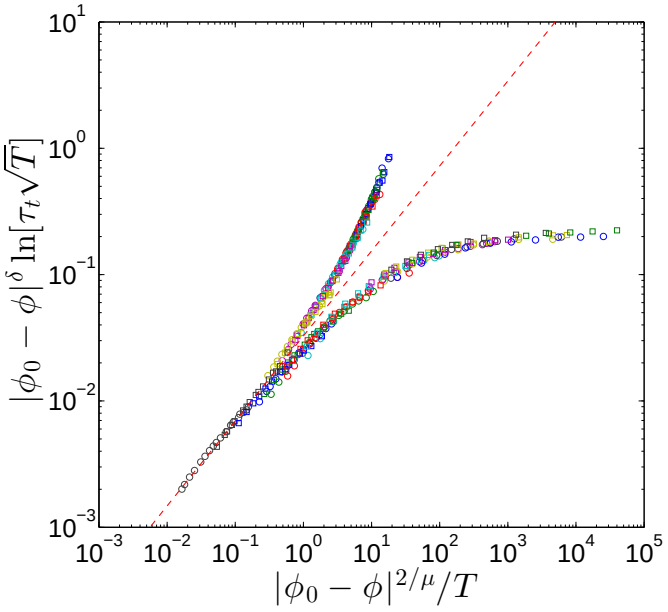

FIG. 17: (Color online) Scaled structural relaxation times for the translational degrees of freedom $|\phi_0 - \phi| \ln \tau_t \sqrt{T}$ versus the scaled temperature $|\phi_0 - \phi|^{2/\mu}/T$ on a ln-ln scale for dimers at $\alpha = 1.3$ for $N = 64$ (squares) and 200 (circles) particles. The system-size dependence of the scaling parameters is weak: $\phi_0 = 0.878$ (0.876); $\mu = 1.23$ (1.25); and $\delta = 1.1$ (1.1) for $N = 256$ (64) particles. The dashed line has slope $\mu\delta/2$ for $N = 256$.

Tables

	μ	δ	$m(\phi_0)$	ϕ_0	ϕ_J^f	ϕ_J^s
2D	1.25 ± 0.04	1.9 ± 0.1	1.19 ± 0.10	0.831 ± 0.005	0.838	0.851
3D	1.3	2.2 ± 0.2	1.43 ± 0.13	0.635 ± 0.005	0.648	0.662

TABLE I: Dynamic scaling exponents μ and δ obtained from fitting the structural relaxation time $\tau_t(\phi, T)$ for the translational degrees of freedom to the form in Eq. 7, fragility $m(\phi_0) = \mu\delta/2$ of structural relaxation at ϕ_0, and the packing fractions ϕ_0, ϕ_J^f, and ϕ_J^s for dense liquids composed of bidisperse, purely repulsive disks in 2D and spheres in 3D [5].